Petroleum and Coal

TPO-GC AND TG-DTA INVESTIGATION OF DRY DECOKING PROCESS IN OLEFIN PLANTS

Farhad Ghadyanlou and Ahmad Azari*

Faculty of Petroleum, Gas, and Petrochemical Engineering (FPGPE), Persian Gulf University (PGU), P.O. Box 75169-13817, Bushehr, Iran

Abstract

The aim of this work is to investigate the combustion mechanism of catalytic coke formed in the olefin plants furnaces as a chemical reaction fouling. The objectives are removing the steam injection and modeling a dry oxidation process based upon Thermogravimetry (TG) and Temperature-Programmed Oxidation-Gas Chromatography (TOP-GC) experiments. Comprehensive data were obtained for 5.0-15.0 % vol. oxygen content in the combustion atmosphere while the temperature was tuned from 600 to more than 1000°C. The concentrations of carbon monoxide and carbon dioxide were determined as TPO criteria for reaction rate and kinetic parameters along with the mass loss in TG tests. The results revealed the optimum decoking temperature in order to decrease the decoking run-time, improve energy conservation and enhance the cleaning efficiency. DTG thermogram revealed the temperatures that the combustion rate of catalytic coke increased gradually. TPO-GC experiments approved the optimal decoking temperature in accordance with the plant's operation manual. The propounded dry decoking mechanism depicted the combustion reaction of carbon and CO_2 follows by O_2 chemisorption at carbon surface, obtaining the activation energy, converting to the activated complex and production of CO_2.

Keywords: *Combustion; Coke; Oxidation; Pyrolysis; Furnace; Modeling, Parametric Study.*

1. Introduction

Steam cracking of hydrocarbons is one important process of the petrochemical industry for olefin production. Carbon deposition phenomena or coke formation deposit on the inner wall of coils is carbonaceous material that results of undesirable side reactions in steam cracking process and a major concern that limits run the length of the furnace in ethylene plants [1-2]. There is a numerous investigation on the mechanisms of carbon deposition under various conditions [1-12]. Generally, there are three categories of coke formation are as the following:

a. Catalytic coke with the filamentous structure of carbonaceous deposition as shown in Figure 1. is results of heterogeneous reaction where occur on the metal surface's active sites (Cr, Ni, Co) and generally doing main role in radiant coil coking in furnaces [1-2, 10, 13].

b. Pyrolytic or gas phase coke deposition occurs by a radical mechanism where procurators joint with existing carbon layer and due to the growth of coke.

c. Coke formation by condensation mechanism is amorphous structure and happens in the low temperature sections [1, 3, 14].

Coke is poor heat conductor, and due to reducing heat transfer rate from flue gas to process gas in coils, increase pressure drop by growing coke layer and reducing cross section of coil, lower ethylene yield and heat input increased if the feed conversion maintained constant then coil skin temperature, gradually increased until reaches design temperature of reactor tube and finally cause to shut-down the furnace for coke removing during burning-off carbonaceous deposition via controlled combustion where carried out by means of a steam/air mixture [1, 3, 12-13].

The amount of coke accumulation depends on feed characteristics, operating severity, the material of coil, run length and the addition of inhibitors [10, 12].
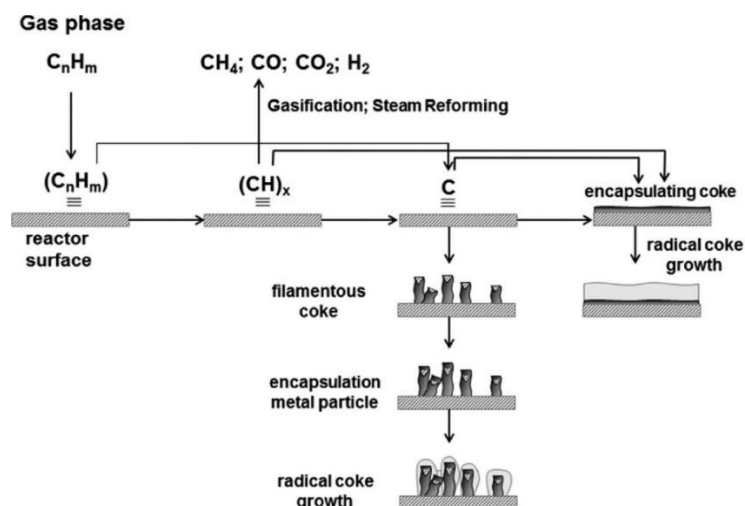

Figure 1. Catalytic coke formation mechanism [15]

There are two alternative industrial decoking technologies exist currently for coke removal that difference of them is end points of decoke effluent. Effluent can be sent to decoke drum or injecting to from bottom or either to the lower end walls of firebox by symmetrical piping configuration for keep particle emissions below 50 mg/Nm^3 during decoke which the second one applied in modern furnaces [16]. Optimization of decoke operation is one of the main interests from the point of view of energy consumption and time of production loss reduction in olefin plants; therefore, it is necessary to determine the mechanisms of coke combustion reactions by real-time analyzing of the deposited coke produced in industrial plants [6].
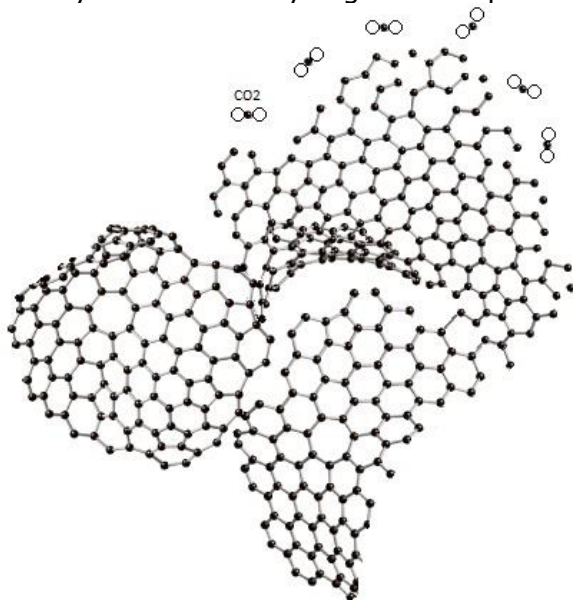
Coke combustion is assigned as a de-volatilization process followed by the combustion of residual coke [17-19] along with the side reaction of gasification [20-22]. The combustion behavior of fine [23] and coarse [24-27] coal particles in the N_2/O_2 atmosphere was studied, and a model was propounded based on devolatilized products and heat-mass transfer phenomena was propounded. In the process of combustion, the carbon atoms in the coke structure react with surrounded oxygen from the point of weak bonds as depicted in Figure 2.

Figure 2. Graphical implementation of coke decomposition in combustion phenomena

The process of various cokes oxidation or combustion has been largely investigated in the field of heterogeneous catalysts [28-30], pulverized coal [31], mineralogical coal [32], coal chars [33], boiler coal [34] and mineral coal [35].

There are many investigations reported by different researchers on various carbonaceous materials gasification and combustion like coal, coal char, coke, petcoke, sewage sludge char [36-61], biomass [62-73], coal-biomass blends [74-75] and municipal solid wastes [76-78]. Some of

the alternative reaction kinetics used by different workers illustrated in Table 1 and there are excellent reviews available which can consider on gasification and combustion of coal and chars [22, 79-85], carbon based deposits [86], municipal solid waste [87] and carbonaceous adsorbents [88-89] and Biomass [90-95].

Table 1. Various reaction mechanisms for carbonaceous material gasification and combustion kinetics by various researchers

Authors	Type of carbonaceous material	Weight (g)	Reaction model	Exp. instrument	T, ºC	Ref.
Jelemensky et al.	Coal char	0.002-0.003	$C + O_2 \rightarrow CO_2$ $C + CO_2 \rightarrow 2CO$ $C + 0.5O_2 \rightarrow CO$ $CO + 0.5O_2 \rightarrow CO_2$	TG	amb.-800	[96]
Keskitalo et al.	Coke of a Ferrierite Catalyst	0.01	$C + 0.5O_2 \rightarrow CO_g$ $C + O_2 \rightarrow CO_{2g}$	TPO-GC	amb.-850	[97]
Gil et al.	Coal and pine sawdust	0.05	A (solid) → B (char) + C1 (gas) B (char) → C2 (gas) + D (ash)	TG-DTG	amb.-615	[98]
Micco et al.	Coal	0.10,0.16,0.30	$C_{(s)} + CO_{2(g)} \leftrightarrow 2CO_{(g)}$	drop tube furnace (DTF)	825- 920	[99]
Nakasaka et al.	Coked MFI-type zeolite	0.1	$C_{(s)} + 0.5O_{2(g)} \rightarrow CO_{(g)}$ $C_{(s)} + O_{2(g)} \rightarrow CO_{2(g)}$ $H + 0.25O_{2(g)} \rightarrow 0.5H_2O$	fixed-bed flow reactor, TG	550-650	[100]
Li et al.	Coal	0.005	$C + CO2 \leftrightarrow 2CO$	TPO-TG	amb.-1450	[101]
Mandapati et al.	Coal char	0.01	$C + CO_2 \rightarrow C(O) + CO$ $C(O) + CO \rightarrow C + CO_2$ $C(O) \rightarrow C + CO$	TG	amb.-1000	[102]
Zhang and et al.	Coal	0.1	$Coal + O_2 \rightarrow Coal - X - O_2 \rightarrow X$ transformation) X denotes the five elements in coal	TGA	<200	[103]
Jing et. al.	Coal	0.005	$C + CO_2 \leftrightarrow C(O) + CO$ $C(O) + C \rightarrow CO + C_f$	TG	amb.-1300	[104]
Veca et al.	Coal char	0.2-0.3	$C + CO2 \rightarrow 2CO$	TGA	800-1100	[105]
Urych	Coal	0.2-0.3	Coal → x (volatiles) + (1 − x) (char) x – the fraction of volatiles	TGA/DSC	298-1173	[106]
Veca & Adrover	Coal char	0.02-0.03	$C + CO_2 \leftrightarrow 2CO$	TG	800-1000	[105]
Nunes et al.	Coal	0.03	$C + O_2 \rightarrow C(O)$ $C(O) \rightarrow CO$	TG	1173K	[107]
Ding et al.	Coal char and petroleum coke char	0.008	$C + H_2O \leftrightarrow CO + H_2$ $CO + H_2O \leftrightarrow CO_2 + H_2$ $C + CO_2 \leftrightarrow 2CO$	drop tube furnace (DTF)-TG	1100-1400	[108]
Chen et al.	Coal	0.3	$C + CO_2 \leftrightarrow CO + C(O)$ $C(O) \leftrightarrow CO + C$ and $C + H_2O \leftrightarrow H_2 + C(O)$ $C(O) \leftrightarrow CO + C$	TG	1173-1273K	[109]
Tanner et al.	Coal	0.01-0.015	$C + CO_2 \leftrightarrow 2CO$ $C + H_2O \leftrightarrow CO + H_2$	drop tube furnace (DTF)-TG	600-1100	[110]
Czerski et. al.	Coal	0.46	$C + CO2 \leftrightarrow 2CO$	TG	Amb-1100	[111]
Liu et al.	coal char	0.5	C + CO2 ↔ C(O) + CO C(O) →CO	HP TG	1050	[112]

The coke removal with decoking process reported in six heterogeneous and homogeneous reactions by Y. Zhang et al. [113] as Eqs. 1-6:

$$C_{(s)} + O_{2(g)} \leftrightarrow CO_{2(g)} \tag{1}$$

$$C_{(s)} + H_2O_{(g)} \leftrightarrow CO_{(g)} + H_{2(g)} \tag{2}$$

$$C_{(s)} + 0.5O_{2(g)} \leftrightarrow CO_{(g)} \tag{3}$$

$$CO_{(g)} + 0.5O_{2(g)} \leftrightarrow CO_{2(g)} \tag{4}$$

$$C_{(s)} + CO_{2(g)} \leftrightarrow 2CO_{(g)} \tag{5}$$

$$CO_{(g)} + H_2O_{(g)} \leftrightarrow CO_{2(g)} + H_{2(g)} \tag{6}$$

Heynderickx *et al.* [14] assumed coke is burning off phenomena undergoing with two fundamental endothermic gasification and oxidation reactions mechanism (*Eq.1*) and (*Eq.2*). In this study investigation was undertaken involving dry oxidation, therefore, reactions (*Eq.2*) and (*Eq.6*) is discarded. Boudouard reaction (*Eq.5*) ignored in addition because the ratio of CO to CO_2 decrease with increasing temperature and carbon monoxide convert to carbon dioxide rapidly. Finally, the set of reactions reduced to *Eqs.* 1, 3, 4 that enthalpies of formation at 298K respectively are as the following [113-115].

$$\Delta H_{R1} = -394 \; kJ/mol \tag{7}$$

$$\Delta H_{R3} = -110 \; kJ/mol \tag{8}$$

$$\Delta H_{R4} = -284 \; kJ/mol \tag{9}$$

Coke thickness (3 cm)
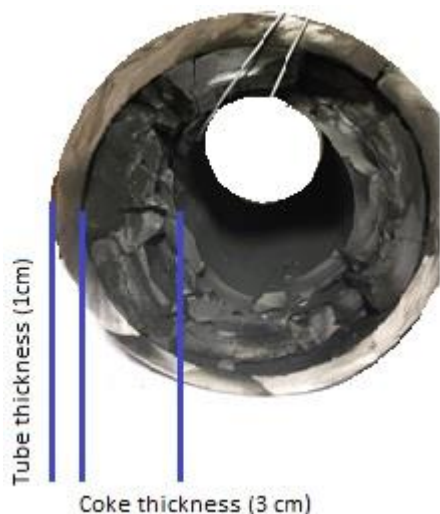
This work aimed to study the combustion characteristics of catalytic coke formed in the furnaces of an olefin plant which extract from a real piece of the coked coil that showed in Figure 3. For this purpose, the coke samples were combusted in a fixed bed tubular reactor under different O_2/N_2 atmospheres from 600 to 1000°C, and coke characters were identified by TG/DTG (Thermogravimetry/Differential Thermogravimetry) analysis and the TPO-GC experiments were conducted under non-isothermal conditions at controlled O_2/N_2 rates.

Figure 3. The cross-section of a piece of the radiant coil with inner wall coke deposit

The main objective was the development of a combustion model for nonporous catalytic coke based upon the weight percent of oxygen.

2. Experimental method

2.1. Materials and chemicals

Coke samples used in experiments were obtained from a piece of radiation coil of an ethane cracker furnace as shown in Figure 3 where were milled in the size of 1-2 mm and Table 2 illustrated the components of this coke.

Table 2. Components of catalytic coke

Test name	Test Method	Percent wt.
Ash	ASTM D3174-11	0.8
Volatile	ASTM D3175-11	0.5
Fixed C	ASTM D3172-89(02)	98.4
Sulfur	ASTM E1915-09	0.1

2.2. Experimental set-up

A horizontal cylindrical reactor with accessory equipment was heated in a digital furnace in the temperature range of 600-1000°C. The reactor was fed by air and nitrogen gasses while

the gas flows were determined and controlled by mass-flow meters (brooks, 5850S, USA) in the range of 10 to 100 mL/min. The reactor tube was manufactured by a thermal resistant metal alloy (SS-304) with a diameter of 15 mm and a length of 200 mm, and experiments were carried out with coke samples located in a reactor tube. The sides of the reactor tube were blinded two four-neck flanges after the coke loading. The temperatures of the furnace, representing the reactor temperature and the flow of inlet gas streams were recorded by a PC system. The effluent gas was analyzed by gas chromatography equipped along with the released gas stream. Figure 4 shows the schematic of the experimental setup.
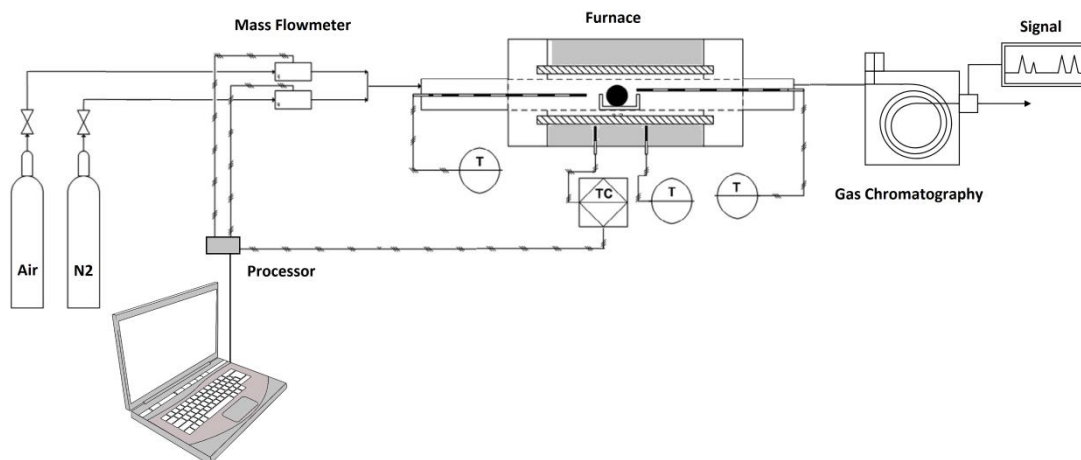

Figure 4. Schematic of TPO-GC set up

Gas chromatography runs were performed by a gas chromatograph (CP3800, Varian, USA) and He carrier gas (BOC, CP grade). The runs were carried out on 1.0 cm^3 fluent gas from the furnace in splitless mode, injector-temperature of 150ºC and pressure of 15.0 psi. The packed column consisted of HAYESEP Q (80-100 mesh) with dimensions of 2 m × 1/8 inch OD × 2.0 mm internal diameters. The column temperature was set at 30°C for 4 min. The TCD filament temperature was set at 200°C.

The coke characteristics were determined by thermogravimety (TG) analyzer (209F1, Netszch, Germany) to obtain TG and DTG traces of the pyrolytic coke samples. The atmosphere was set on ambient air, and the flow rate was fixed on 25 mL/min. The sample weight was selected to be 50-100 mg heated in the range of 30-900°C by the ramp of 20°C/min in an alumina-pan. Data was compiled and processed by Proteus Analysis Software.

2.3. Characteristic tests

The samples of catalytic coke, which accurately were weighted to 100 mg, were dried at 100°C for 20 min, then it was heated at a constant rate (ramp) of 20°C/min from 100°C to 600°C under air atmosphere (100 mL/min), then held at 1000°C for 10 min to complete de-volatilization step. After that, the air stream (100 mL/min) was injected and the temperature decreased to ambient.

2.4. Combustion procedure

The TPO experimental setup, which has been depicted schematically in Figure 4, was a tubular reactor located in the thermostatically-controlled furnace. The reactor was loaded by 190, 138 and 501 mg of catalytic coke samples for combustion studies. The reason why the small quantity of coke was used is to ensure the exothermicity combustion reactions and the endothermicity cracking reactions do not fluctuate the temperature of the reactor bed. The temperature was increased from the ambient conditions to 600°C (20°C/min), from 600°C to 800°C (10°C/min), from 800°C to 1000°C (5°C/min) and hold at 1000°C for 10 min. The temperatures were monitored by thermocouples placed around the reactor, and the pressure was fixed by pressure regulators at the outlet stream to the combustion-reactor. Along with the

reaction, the effluent gas stream passed through a sampling valve of gas chromatography resulted in the online determination of concentrations of carbon monoxide and carbon dioxide products. After the experiments, the residual coke in the reactor was flushed-out with nitrogen (100 mL/min) until 100°C. These residues were collected and weighted by analytical balance (Kern, Germany). The weight losses of residue samples of runs 1-3 were determined, and the results are depicted in Table 3.

Table 3. The weight loss of residue samples of runs 1-3

Run	Primary weight (mg)	Secondary weight (mg)	Weight loss (%)
1	190	80	58
2	138	70	49
3	501	230	54

3. Results and discussions

3.1. TG Experimental results

TG experiment at air atmosphere was conducted, and the results are presented in Figure 5.
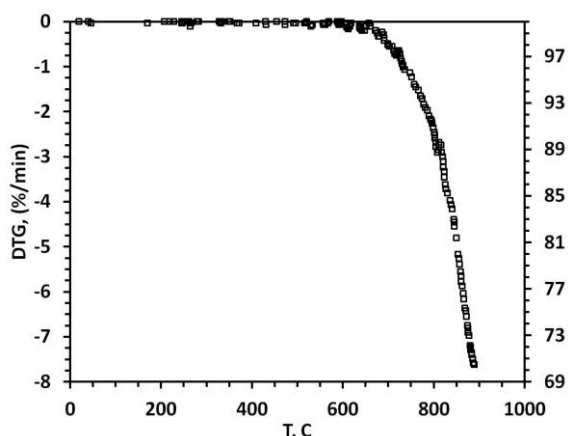

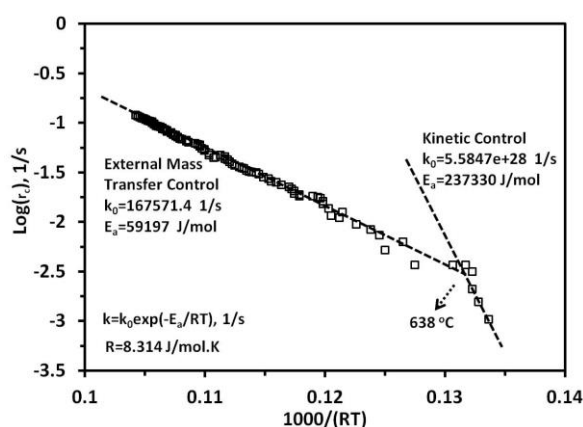Figure 5. TG and DTG diagrams of catalytic coke

Figure 6. Arrhenius diagram of coke oxidation-change of rate step control

The combustion started at 700°C, and its rate was maximized at 900°C leading to a 30% decrease in the mass of the coke. The nonporous structure of catalytic coke shows a smooth line in the temperatures less than 700°C since no trapped or adsorbed hydrocarbons and water were released, and no mass-loss was recorded. DTG curve highlighted that from 700°C to 900°C the combustion rate increases gradually.

Figure 6 drew regarding TG data and Arrhenius relationship and mass basis rate of combustion formula:

$$r_c = -\frac{1}{m}\frac{dm}{dt} \qquad (10)$$

Slope changes at nick point in this figure indicate how the mechanisms controlled the rate of combustion. At the lower temperatures than 638°C the controlling mechanism is kinetic control, and at the higher temperatures than 638°C diffusion is controlling step which frequency coefficient and activation energies in these steps are 5.5847e+28, 167571.4 s^{-1} and 237330 ,59197 J.mol^{-1}, respectively and finally, rates of combustion in these mechanisms defined as the following *Eqs.* while R=8.314 J/mol.K.

$$r_c = 5.58 \times 10^{28} \, exp\left(\frac{-237330}{RT}\right) \qquad (11)$$

$$r_c = 167571.4 \, exp\left(\frac{-59197}{RT}\right) \qquad (12)$$

3.2. Combustion mechanism of decoking

As discussed before, the combustion phenomena of catalytic coke were assessed experimentally under an oxygen atmosphere (5.0, 10.0 and 15.0 % vol.) and at different temperatures (600-1000°C) as their results presented in Table 4.

Table 4. Characteristics of experimental runs

Run	Oxygen (% *Vol.*)	Time (min)	T (°C)	C_{CO2} (% *wt.*)
1	5	0	600	0.1953
		10	700	0.1683
		20	800	0.0782
		30	850	0.7680
		40	900	0.1547
		50	950	0.3920
		60	1000	0.2419
2	10	0	600	0.1359
		10	700	0.1121
		20	800	0.1170
		27	835	0.1731
		30	850	0.1318
		40	900	0.1062
		50	950	1.0883
		60	1000	0.3389
		70	1010	0.1192
3	15	0	600	0.0873
		10	700	0.0704
		20	800	0.2393
		27	835	0.0852
		30	850	2.2566
		40	900	0.2957
		50	950	0.6548
		60	1000	0.2700
		70	1010	0.1517

It is clearly obvious that the oxygen chemisorptions more in temperatures lower than 850°C in 1 and 3 runs and at the lower than 950°C in step 2 as seen in Table 4 and rapid CO_2 formed desorption in 850°C and 950°C at 1, 3 and 2 runs, respectively occur due to oxygen chemisorbbed before. The experimental results depicted that the maximum CO_2 concentration was determined at 850°C in with 5 and 15 vol.% of oxygen concentrations media and at 950°C in respect to 10 vol.% which are in accordance with the field data for gas-feed olefin furnaces.

According to the results of Table 4, by increasing the temperature along with time, the concentration of produced CO_2 is changed because of the revolution of surface phenomena including adsorption of O_2 at carbon surface, formation of activated complexes of C–C–O, breaking the C–C bonds and release of CO_2. The results of Table 4 were graphically implemented in Figure 7 to explain the decoking process based on the released concentration of CO_2.

The main concentrations of the released CO_2 are attributed to two temperatures of 850 and 950°C. The areas behind the traces, which reveal the overall production of CO_2 along with temperature rise, represent that CO_2 production at O_2 concentration of 15% vol. was twice than that of for both O_2 concentrations of 5 or 15% vol. Moreover, it is obvious that combustion reactions are conducted at two temperature regions of 800-900°C and 900-1000°C, with a quench temperature of Q~900°C in which the decoking reactions are assigned to be quenched.

The orders of CO_2 production at two decoking regions of 800-900°C and 900-1000°C are not identical because of different decoking mechanisms.

In the region of 800-900°C, the magnitude of CO_2 production follows as O_2 concentrations of 10% < 5% << 15%. On the other hand, in the region of 900-1000°C, that magnitude follows as 5% < 15% < 10% vol. O_2.
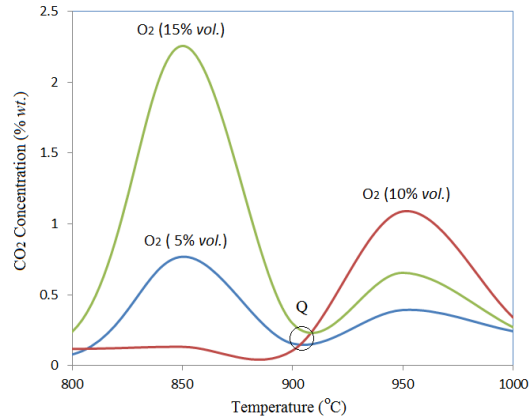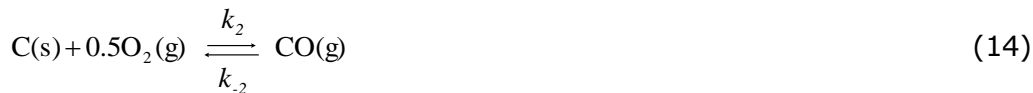
Figure 7. Comparative production of CO2 at different O2 concentrations and elevated temperatures

A combustion mechanism was propounded based upon the supposed reactions, which are assigned to occur in these conditions, and the results were matched with the experimental data gathered from TPO tests. Eqs. 1, 3 and 4 were proposed as the mechanism of these reactions as the following:

$$C(s) + O_2(g) \underset{k_{-1}}{\overset{k_1}{\rightleftharpoons}} CO_2(g) \tag{13}$$

$$C(s) + 0.5O_2(g) \underset{k_{-2}}{\overset{k_2}{\rightleftharpoons}} CO(g) \tag{14}$$

$$CO(g) + 0.5O_2(g) \underset{k_{-3}}{\overset{k_3}{\rightleftharpoons}} CO_2(g) \tag{15}$$

Respect to *Eqs.* 13, 14 and 15 and with the assumption of elementary reactions, the reaction rate of CO2 (r_{CO2}) production is determined as *Eq.* 16.

$$r_{CO_2} = k_1 C_{O_2} - k_{-1} C_{CO_2} + k_3 C_{CO}.C_{O_2}^{1/2} - k_{-3} C_{CO_2} \tag{16}$$

where: k_1, k_{-1}, k_2, k_{-2}, k_3, and k_{-3} represent the rate constants of reactions *Eqs* 13, 14 and 15, respectively. C_{O2}, C_{CO}, and C_{CO2} show the concentration of oxygen, carbon monoxide and carbon dioxide gases as %*wt*.

Due to this fact that CO is intermediate; therefore, the concentration gradient with respect to time is assumed to be zero. Hence, according to the steady state hypothesis, the rate of CO reactions and its concentration is determined by *Eqs. 17* and *18*, respectively.

$$+r_{CO} = k_2 C_{O_2}^{1/2} - k_{-2} C_{CO} - k_3 C_{CO}.C_{O_2}^{1/2} + k_{-3} C_{CO_2} = 0 \tag{17}$$

$$C_{CO} = \frac{k_2 C_{O_2}^{1/2} + k_{-3} C_{CO_2}}{k_{-2} + k_3 C_{O_2}^{1/2}} \tag{18}$$

In addition, GC reports revealed that the concentration of CO is determined to be negligible in the reaction atmosphere

By replacing *Eq. 18* in *Eq. 16* and simplification, *Eq. 19* is obtained.

$$-r_{CO_2} = \left[\frac{(k_1 k_{-2} + k_2 k_3) C_{O_2} + k_1 k_3 C_{O_2}^{3/2}}{k_{-2} + k_3 C_{O_2}^{1/2}} \right] - \left[\frac{k_{-1} k_{-2} + k_{-1} k_3 C_{O_2}^{1/2} + k_{-2} k_{-3}}{k_{-2} + k_3 C_{O_2}^{1/2}} \right] C_{CO_2} \tag{19}$$

According to the above-listed k_n values, *Eqs*. 20 and 21 are given.

$$k_2 k_3 >> k_1 k_{-2} \tag{20}$$

$$k_{-2} << k_3 C_{O_2}^{1/2} \tag{21}$$

Therefore, in the first assumption of this developed model, the $k_1 k_{-2}$ is negligible with respect to the $k_2 k_3$ of *Eq*. 19 and it can be neglected. Likewise, in the second assumption of the model, the $k_{-1} k_{-2}$ and $k_{-2} k_{-3}$ are negligible with respect to the left term ($k_{-1} k_3 C_{O_2}^{1/2}$) of *Eq*. 19. Therefore, the rate of reaction (*Eq*. 19) is written as *Eq*. 22.

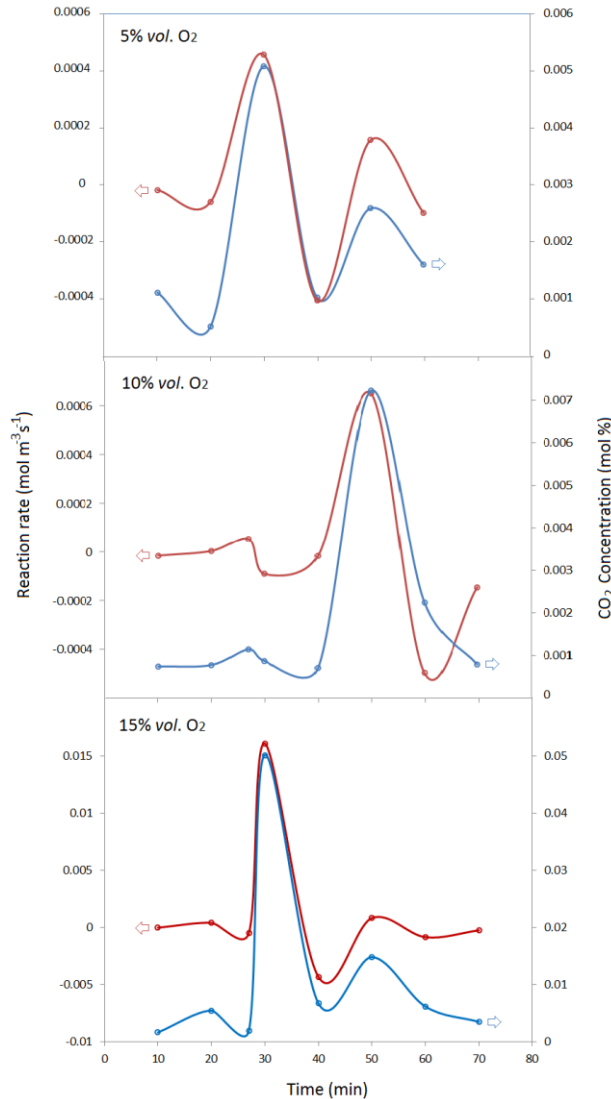$$r_{CO_2} = (k_2 C_{O_2}^{1/2} + k_1 C_{O_2}) - k_{-1} C_{CO_2} \tag{22}$$

Figure 8. Reaction rate and CO_2 concentration of dry decoking in different O_2 concentrations of combustion atmosphere

The developed model reveals that the overall rate constant is a function of the concentrations of oxygen and carbon dioxide. Therefore, it is possible to determine the overall rate constant of combustion reaction using the concentrations of oxygen and carbon dioxide in the combustion atmosphere.

The experimental data obtained from the combustion of catalytic coke and they were fitted to Eq. 22 in order to assess the accuracy of the proposed mechanism (Table 4).

The graphical illustration of the experimental data is depicted in Figure 7 representing a positive reaction rate when the CO_2 concentration increases and vice versa. Therefore, the bi-functional Eq. 22 is used to admit the variation of reaction signs.

The positive reaction rate at the increased CO_2 concentration is attributed to high concentration of O_2 in the combustion reaction leading to increasing the first term of Eq. 22, means moving to more positive values. On the other hand, when the CO_2 concentration decreases, the reaction rate moves to the negative values since the reaction of carbon to CO_2 follows by adsorption of O_2 at carbon surface, obtaining the activation energy, converting to the activated complex and production of CO_2.

Therefore, at descending concentration of CO_2, the carbon surface is going to adsorb O_2 and cannot react to it since the concentration of activated complex is low. At these conditions, the first term of Eq. 22 is reduced with respect to the second term, and the overall sign is negative.

The above discussions and the trend of Figure 8 were in accordance with three oxygen concentrations (5, 10 and 15% vol.) of combustion atmosphere, approving the proposed mechanism.

4. Conclusions

Dry oxidation of deposited catalytic coke on the coil surfaces of an ethane cracker furnace was studied by TG/DTA, and TPO-GC techniques and the main conclusions were drown are

1- Arrhenius diagram analysis showed a change in controlling steps of combustion rate occurs at around $640^{\circ}C$ (break point).
2- DTG thermogram revealed that in the range of 700-900°C the combustion rate of catalytic coke increased gradually. The maximum combustion rate was determined by TPO-GC experiments to be at $850^{\circ}C$, which is in accordance with the plant's operation manual.
3- The positive reaction rate at the increased CO_2 concentration is attributed to high concentration of O_2 in the combustion reaction leading to moving the reaction rate to more positive values.
4- The proposed mechanism depicted that the combustion reaction of carbon and CO_2 follows by chemisorption of oxygen at carbon surface, obtaining the activation energy, converting to the activated complex and production of CO_2.
5- At the concentration of 5% and 15 % vol. oxygen and lower temperatures than $850^{\circ}C$, the rate of O_2 chemisorption is higher, and the rate of carbon monoxide formation is more in $850^{\circ}C$, and it similarly occurs for the concentration of 10 % vol, at $950^{\circ}C$. It is demonstrated that burning off coke in decoking of steam cracker furnaces is optimized by TG/DTA and TPO TPO-GC techniques usage leading to more energy conservation.

Acknowledgements

References

[1]   Browne J, Broutin P, and Ropital F. Coke deposition under steam cracking conditions – Study of the influence of the feedstock conversion by micropilots experiments. Materials and Corrosion. 1998; 49(5): 360–366.
[2]   Cai H, Krzywicki A, and Oballa MC. Coke formation in steam crackers for ethylene production. Chemical Engineering and Processing: Process Intensification. 2002; 41(3): 199-214.
[3]   Abghari SZ. Investigation of Coke Formation in Steam Cracking of Atmospheric Gasoil. Journal of Petroleum Science Research (JPSR). April 2013; 2(2): 82-91.
[4]   Kopinke FD, Zimmermann G, and Nowak S. On the mechanism of coke formation in steam cracking—conclusions from results obtained by tracer experiments. Carbon. 1998; 26(2): 117-124.
[5]   Reyniers GC, Froment GF, Kopinke F-D, and Zimmermann G. Coke Formation in the Thermal Cracking of Hydrocarbons. 4. Modeling of Coke Formation in Naphtha Cracking. Ind. Eng. Chem. Res. 1994; 33(11): 2584–2590.
[6]   Kopinke FD, Zimmermann G, Reyniers GC, and Froment GF. Relative rates of coke formation from hydrocarbons in steam cracking of naphtha. 2. Paraffins, naphthenes, mono-, di-, and cyclo-olefins, and acetylenes. Ind. Eng. Chem. Res. 1993; 32(1): 56–61.
[7]   Wang J, Reyniers M-F, and Marin GB. Influence of dimethyl disulfide on coke formation during steam cracking of hydrocarbons. Ind. Eng. Chem. Res. 2007; 46 (12): 4134–4148.
[8]   Alselaa RAM and Elfghi FM. Reduction of coke accumulation and energy resources by adding steam and carbon dioxide in naphtha based ethylene production. Chemical and Process Engineering Research. 2014; 28: 21 –31.
[9]   Chan KYG, Inal F, and Senkan S. Suppression of Coke Formation in the Steam Cracking of Alkanes: Ethane and Propane. Ind. Eng. Chem. Res. 1998; 37(3): 901–907.
[10]   Jambor B and Hajekova E. Formation of coke deposits and coke inhibition methods during steam cracking. Pet Coal, 2015; 57(2): 143-153.
[11]   Vandewalle LA, Van Cauwenberge DJ, Dedeyne JN, Van Geem KM, and Marin GB. Dynamic simulation of fouling in steam cracking reactors using CFD. Chemical Engineering Journal. 2017; 329:77-87.
[12]   Kucora I, Paunjoric P, Tolmac J, Vulovic M, Speight JG, and Radovanovic L. Coke formation in pyrolysis furnaces in the petrochemical industry. Petroleum Science and Technology. 2017; 35(3): 213-221.

[13]   Heynderickx GJ and Froment GF. Simulation and Comparison of the Run Length of an Ethane Cracking Furnace with Reactor Tubes of Circular and Elliptical Cross Sections. Industrial & Engineering Chemistry Research. 1998; 37(3): 914-922.

[14]   Heynderickx GJ, Schools EM, and Marin GB. Simulation of the decoking of an ethane cracker with a steam/air mixture. Chemical Engineering Science. 2006; 61(6): 1779-1789.

[15]   Muñoz Gandarillas AsE, Van Geem KM, Reyniers M-Fo, and Marin GB. Influence of the reactor material composition on coke formation during ethane steam cracking. Industrial & Engineering Chemistry Research. 2014; 53(15): 6358-6371.

[16]   Enqvist KJ, Oy BP, Torpe D, Noretyl A, and Middleton J. Dust Emissions during Cracking Furnace Decoking–Regulations Versus the Measured Performance. in 2008 Spring National Meeting. 2008.

[17]   Essenhigh RH, Misra MK, and Shaw DW. Ignition of coal particles: a review. Combustion and Flame. 1989; 77(1): 3-30.

[18]   Liu X, Xu M, Si J, Gu Y, Xiong C, and Yao H. Effect of sodium on the structure and reactivity of the chars formed under N_2 and CO_2 atmospheres. Energy & Fuels. 2011; 26(1): 185-192.

[19]   Su S, Song Y, Wang Y, Li T, Hu S, Xiang J, and Li C-Z. Effects of CO_2 and heating rate on the characteristics of chars prepared in CO_2 and N_2 atmospheres. Fuel. 2015; 142: 243-249.

[20]   Xu J, Su S, Sun Z, Qing M, Xiong Z, Wang Y, Jiang L, Hu S, and Xiang J. Effects of steam and CO_2 on the characteristics of chars during devolatilization in oxy-steam combustion process. Applied Energy. 2016; 182: 20-28.

[21]   Yi B-j, Zhang L-q, Yuan Q-x, Yan S-p, and Zheng C-g. The evolution of coal char structure under the oxy-fuel combustion containing high H_2O. Fuel Processing Technology. 2016; 152: 294-302.

[22]   Bhunia S, Sadhukhan AK, and Gupta P. Modelling and experimental studies on oxy-fuel combustion of coarse size coal char. Fuel Processing Technology. 2017; 158: 73-84.

[23]   Maffei T, Khatami R, Pierucci S, Faravelli T, Ranzi E, and Levendis YA. Experimental and modeling study of single coal particle combustion in O_2/N_2 and oxy-fuel (O_2/CO_2) atmospheres. Combustion and Flame. 2013; 160(11): 2559-2572.

[24]   Sadhukhan AK, Gupta P, and Kumar Saha R. Modeling and experimental studies on combustion characteristics of porous coal char: Volume reaction model. International Journal of Chemical Kinetics. 2010; 42(5): 299-315.

[25]   Roy B and Bhattacharya S. Combustion of single char particles from Victorian brown coal under oxy-fuel fluidized bed conditions. Fuel. 2016; 165: 477-483.

[26]   Brix J, Navascués LG, Nielsen JB, Bonnek PL, Larsen HE, Clausen S, Glarborg P, and Jensen AD. Oxy-fuel combustion of millimeter-sized coal char: Particle temperatures and NO formation. Fuel. 2013; 106: 72-78.

[27]   Scala F and Chirone R. Fluidized bed combustion of single coal char particles at high CO_2 concentration. Chemical Engineering Journal. 2010; 165(3): 902-906.

[28]   Nalitham RV, Tarrer AR, Guin JA, and Curtis CW. Kinetics of coke oxidation from solvent refined coal hydrotreating catalysts. Industrial & Engineering Chemistry Process Design and Development. 1985; 24(1): 160-167.

[29]   Le Minh C, Jones RA, Craven IE, and Brown TC. Temperature-programmed oxidation of coke deposited on cracking catalysts: combustion mechanism dependence. Energy & fuels. 1997; 11(2): 463-469.

[30]   Sánchez B, Gross MS, Dalla Costa B, and Querini CA. Coke analysis by temperature-programmed oxidation: Morphology characterization. Applied Catalysis A: General. 2009; 364(1): 35-41.

[31]   Wang G-w, Zhang J-l, Shao J-g, Hui S, and Zuo H-b. Thermogravimetric analysis of coal char combustion kinetics. Journal of Iron and Steel Research, International. 2014; 21(10): 897-904.

[32]   Everson RC, Neomagus HW, van der Merwe GW, Koekemoer A, and Bunt JR. The properties of large coal particles and reaction kinetics of corresponding chars. Fuel. 2015; 140: 17-26.

[33]   Zhang L, Zou C, Wu D, Liu Y, and Zheng C. A study of coal chars combustion in O_2/H_2O mixtures by thermogravimetric analysis. Journal of Thermal Analysis and Calorimetry. 2016; 126(2): 995-1005.

[34]   McConnell J, Goshayeshi B, and Sutherland JC. An evaluation of the efficacy of various coal combustion models for predicting char burnout. Fuel. 2017; 201: 53-64.

[35]   Zeng X, Zheng S, Zhou H, Fang Q, and Lou C. Char burnout characteristics of five coals below and above ash flow temperature: TG, SEM, and EDS analysis. Applied Thermal Engineering. 2016; 103: 1156-1163.

[36]   Hull AS and Agarwal PK. Estimation of kinetic rate parameters for coal combustion from measurements of the ignition temperature. Fuel. 1998; 77(9-10): 1051-1058.

[37]   Cozzani V. Reactivity in oxygen and carbon dioxide of char formed in the pyrolysis of refuse-derived fuel. Industrial & engineering chemistry research. 2000; 39(4): 864-872.

[38]   Žajdlík R, Remiarová B, and Markoš J. Experimental and modelling investigations of single coal particle combustion. Chemical Engineering Science. 2001; 56(4): 1355-1361.

[39]   Struis R, von Scala C, Stucki S, and Prins R. Gasification reactivity of charcoal with CO_2. Part I: Conversion and structural phenomena. Chemical Engineering Science. 2002; 57(17): 3581-3592.

[40]   Everson R, Neomagus H, and Kaitano R. The modeling of the combustion of high-ash coal–char particles suitable for pressurised fluidized bed combustion: shrinking reacted core model. Fuel. 2005; 84(9): 1136-1143.

[41]   Everson RC, Neomagus HW, and Njapha D. Kinetic analysis of non-isothermal thermogravimetric analyser results using a new method for the evaluation of the temperature integral and multi-heating rates. Fuel. 2006; 85(3): 418-422.

[42]   Yang H, Chen H, Ju F, Yan R, and Zhang S. Influence of pressure on coal pyrolysis and char gasification. Energy & Fuels. 2007; 21(6): 3165-3170.

[43]   Wu Y, Wu S, Gu J, and Gao J. Differences in physical properties and CO_2 gasification reactivity between coal char and petroleum coke. Process Safety and Environmental Protection. 2009; 87(5): 323-330.

[44]   Sommariva S, Maffei T, Migliavacca G, Faravelli T, and Ranzi E. A predictive multi-step kinetic model of coal devolatilization. Fuel. 2010; 89(2): 318-328.

[45]   Scala F and Chirone R. Combustion of single coal char particles under fluidized bed oxyfiring conditions. Industrial & Engineering Chemistry Research. 2010; 49(21): 11029-11036.

[46]   Karimi A, Semagina N, and Gray MR. Kinetics of catalytic steam gasification of bitumen coke. Fuel. 2011; 90(3): 1285-1291.

[47]   Hattingh BB, Everson RC, Neomagus HW, and Bunt JR. Assessing the catalytic effect of coal ash constituents on the CO2 gasification rate of high ash, South African coal. Fuel processing technology. 2011; 92(10): 2048-2054.

[48]   Mianowski A, Robak Z, Tomaszewicz M, and Stelmach S. The Boudouard–Bell reaction analysis under high pressure conditions. Journal of thermal analysis and calorimetry. 2012; 110(1): 93-102.

[49]   Senneca O and Cortese L. Kinetics of coal oxy-combustion by means of different experimental techniques. Fuel. 2012; 102: 751-759.

[50]   Nikrityuk PA, Gräbner M, Kestel M, and Meyer B. Numerical study of the influence of heterogeneous kinetics on the carbon consumption by oxidation of a single coal particle. Fuel. 2013; 114: 88-98.

[51]   Yuan L and Smith AC. Experimental study on CO and CO_2 emissions from spontaneous heating of coals at varying temperatures and O2 concentrations. Journal of loss prevention in the process industries. 2013; 26(6): 1321-1327.

[52]   Li P, Yu Q, Xie H, Qin Q, and Wang K. CO_2 gasification rate analysis of Datong coal using slag granules as heat carrier for heat recovery from blast furnace slag by using a chemical reaction. Energy & Fuels. 2013; 27(8): 4810-4817.

[53]   Kenarsari SD and Zheng Y. CO2 gasification of coal under concentrated thermal radiation: A numerical study. Fuel Processing Technology. 2014; 118: 218-227.

[54]   Huo W, Zhou Z, Wang F, and Yu G. Mechanism analysis and experimental verification of pore diffusion on coke and coal char gasification with CO_2. Chemical Engineering Journal. 2014; 244: 227-233.

[55]   Gomez A and Mahinpey N. A new model to estimate CO_2 coal gasification kinetics based only on parent coal characterization properties. Applied Energy. 2015; 137: 126-133.

[56]   Gonzalo-Tirado C and Jiménez S. Detailed analysis of the CO oxidation chemistry around a coal char particle under conventional and oxy-fuel combustion conditions. Combustion and Flame. 2015; 162(2): 478-485.

[57]   Vorobiev N, Geier M, Schiemann M, and Scherer V. Experimentation for char combustion kinetics measurements: bias from char preparation. Fuel Processing Technology. 2016; 151: 155-165.

[58]   Engin B and Atakül H. Air and oxy-fuel combustion kinetics of low rank lignites. Journal of the Energy Institute. 2016.

[59]   Ju Y and Lee C-H. Evaluation of the energy efficiency of the shell coal gasification process by coal type. Energy Conversion and Management. 2017; 143: 123-136.

[60]   JIAO S-h, LIN X-q, GUO A-j, Kun C, WANG Z-x, TONG J-j, GENG Y-x, LI R-m, and LIU Q-h. Effect of characteristics of inferior residues on thermal coke induction periods. Journal of Fuel Chemistry and Technology. 2017; 45(2): 165-171.

[61]   Prabhakar A, Sadhukhan AK, Kamila B, and Gupta P. Modeling and Experimental Studies on CO_2 Gasification of Coarse Coal Char Particle. Energy & Fuels. 2017; 31(3): 2652-2662.

[62]   Fushimi C, Araki K, Yamaguchi Y, and Tsutsumi A. Effect of heating rate on steam gasification of biomass. 2. Thermogravimetric-mass spectrometric (TG-MS) analysis of gas evolution. Industrial & Engineering Chemistry Research. 2003; 42(17): 3929-3936.

[63]   Melgar A, Perez JF, Laget H, and Horillo A. Thermochemical equilibrium modelling of a gasifying process. Energy conversion and management. 2007; 48(1): 59-67.

[64]   Branca C and Di Blasi C. Combustion kinetics of secondary biomass chars in the kinetic regime. Energy & Fuels. 2010; 24(10): 5741-5750.

[65]   Yuan S, Chen X-l, Li J, and Wang F-c. CO2 gasification kinetics of biomass char derived from high-temperature rapid pyrolysis. Energy & Fuels. 2011; 25(5): 2314-2321.

[66]   Umeki K, Moilanen A, Gómez-Barea A, and Konttinen J. A model of biomass char gasification describing the change in catalytic activity of ash. Chemical engineering journal. 2012; 207: 616-624.

[67]   Kok MV and Özgür E. Thermal analysis and kinetics of biomass samples. Fuel processing technology. 2013; 106: 739-743.

[68]   Barisano D, Canneto G, Nanna F, Villone A, Alvino E, Carnevale M, and Pinto G. Production of gaseous carriers via biomass gasification for energy purposes. Energy Procedia. 2014; 45: 2-11.

[69]   Fatehi H and Bai X-S. Effect of pore size on the gasification of biomass char. Energy Procedia. 2015; 75: 779-785.

[70]   Salem AM and Paul MC. Advanced kinetic modelling of biomass gasification based on optimum height of the reduction zone. International Journal of Advances in Science, Engineering and Technology. 2016; 4(3 Sp2): 182-185.

[71]   Bates RB, Altantzis C, and Ghoniem AF. Modeling of biomass char gasification, combustion, and attrition kinetics in fluidized beds. Energy & Fuels. 2016; 30(1): 360-376.

[72]   Jeong HJ, Hwang IS, Park SS, and Hwang J. Investigation on co-gasification of coal and biomass in Shell gasifier by using a validated gasification model. Fuel. 2017; 196: 371-377.

[73]   Wielgosiński G, Łechtańska P, and Namiecińska O. Emission of some pollutants from biomass combustion in comparison to hard coal combustion. Journal of the Energy Institute. 2016.

[74]   Jayaraman K, Kok MV, and Gokalp I. Thermogravimetric and mass spectrometric (TG-MS) analysis and kinetics of coal-biomass blends. Renewable Energy. 2017; 101: 293-300.

[75]   Xu Q, Pang S, and Levi T. Reaction kinetics and producer gas compositions of steam gasification of coal and biomass blend chars, part 2: Mathematical modelling and model validation. Chemical Engineering Science. 2011; 66(10): 2232-2240.

[76]   Collina E, Lasagni M, Tettamanti M, and Pitea D. Kinetics of MSWI fly ash thermal degradation. 2. Mechanism of native carbon gasification. Environmental science & technology. 2000; 34(1): 137-142.

[77]   Couto ND, Silva VB, and Rouboa A. Thermodynamic Evaluation of Portuguese municipal solid waste gasification. Journal of Cleaner Production. 2016; 139: 622-635.

[78]   Liu G, Liao Y, Guo S, Ma X, Zeng C, and Wu J. Thermal behavior and kinetics of municipal solid waste during pyrolysis and combustion process. Applied Thermal Engineering. 2016; 98: 400-408.

[79]   Smith I. The combustion rates of coal chars: a review. in Symposium (International) on combustion. 1982. Elsevier.

[80]   Sun Z-q, Wu J-h, and Zhang D. CO2 and H2O Gasification Kinetics of a Coal Char in the Presence of Methane. Energy & Fuels. 2008; 22(4): 2160-2165.

[81]   Irfan MF, Usman MR, and Kusakabe K. Coal gasification in CO2 atmosphere and its kinetics since 1948: a brief review. Energy. 2011; 36(1): 12-40.

[82]   Slavinskaya NA. Chemical kinetic modeling in coal gasification processes: An overview. GT2010-23362, ASME Turbo Expo 2010. 2010.

[83]   Lahijani P, Zainal ZA, Mohammadi M, and Mohamed AR. Conversion of the greenhouse gas CO2 to the fuel gas CO via the Boudouard reaction: A review. Renewable and Sustainable Energy Reviews. 2015; 41: 615-632.

[84]   Garcia-Nunez JA, Pelaez-Samaniego MR, Garcia-Perez ME, Fonts I, Abrego J, Westerhof RJ, and Garcia-Perez M. Historical Developments of Pyrolysis Reactors: A Review. Energy & Fuels. 2017; 31(6): 5751-5775.

[85]   Hower JC, Groppo JG, Graham UM, Ward CR, Kostova IJ, Maroto-Valer MM, and Dai S. Coal-derived unburned carbons in fly ash: A review. International Journal of Coal Geology. 2017.

[86]   Mahamulkar S, Yin K, Agrawal PK, Davis RJ, Jones CW, Malek A, and Shibata H. Formation and oxidation/gasification of carbonaceous deposits: a review. Industrial & Engineering Chemistry Research. 2016; 55(37): 9760-9818.

[87]   Chhabra V, Shastri Y, and Bhattacharya S. Kinetics of Pyrolysis of Mixed Municipal Solid Waste-A Review. Procedia Environmental Sciences. 2016; 35: 513-527.

[88]   Creamer AE and Gao B. Carbon-based adsorbents for post combustion CO_2 capture: A critical review. Environmental science & technology. 2016; 50(14): 7276-7289.

[89]   Jaramillo J, Álvarez PM, and Gómez-Serrano V. Oxidation of activated carbon by dry and wet methods: Surface chemistry and textural modifications. Fuel Processing Technology. 2010; 91(11): 1768-1775.

[90]   Prakash N and Karunanithi T. Kinetic modeling in biomass pyrolysis–a review. Journal of Applied Sciences Research. 2008; 4(12): 1627-1636.

[91]   Ranzi E, Cuoci A, Faravelli T, Frassoldati A, Migliavacca G, Pierucci S, and Sommariva S. Chemical kinetics of biomass pyrolysis. Energy & Fuels. 2008; 22(6): 4292-4300.

[92]   Abuelnuor A, Wahid M, Hosseini SE, Saat A, Saqr KM, Sait HH, and Osman M. Characteristics of biomass in flameless combustion: A review. Renewable and Sustainable Energy Reviews. 2014; 33: 363-370.

[93]   Rosselló TM, Li J, and Lue L. Kinetic models for biomass pyrolysis. Archives of Industrial Biotechnology. 2016; 1(1).

[94]   Claude V, Courson C, Köhler M, and Lambert SpD. Overview and essentials of biomass gasification technologies and their catalytic cleaning methods. Energy & Fuels. 2016; 30(11): 8791-8814.

[95]   Murillo J, Biernacki J, Northrup S, and Mohammad A. Biomass pyrolysis kinetics: A review of molecular-scale modeling contributions. Brazilian Journal of Chemical Engineering. 2017; 34(1): 1-18.

[96]   Jelemenský Ľ, Markoš J, Žajdlík R, and Remiarová B. Modelling of Nonlinear Behaviour during Combustion of Single Coal Char Particle. Chemical Papers. 2000; 54(6b): 473-481.

[97]   Keskitalo TJ, Lipiäinen KJ, and Krause AOI. Kinetic modeling of coke oxidation of a ferrierite catalyst. Industrial & engineering chemistry research. 2006; 45(19): 6458-6467.

[98]   Gil MV, Casal D, Pevida C, Pis J, and Rubiera F. Thermal behaviour and kinetics of coal/biomass blends during co-combustion. Bioresource Technology. 2010; 101(14): 5601-5608.

[99]   De Micco G, Nasjleti A, and Bohe A. Kinetics of the gasification of a Rio Turbio coal under different pyrolysis temperatures. Fuel. 2012; 95: 537-543.

[100]   Nakasaka Y, Tago T, Konno H, Okabe A, and Masuda T. Kinetic study for burning regeneration of coked MFI-type zeolite and numerical modeling for regeneration process in a fixed-bed reactor. Chemical engineering journal. 2012; 207: 368-376.

[101]   Li P, Yu Q, Qin Q, and Lei W. Kinetics of CO_2/Coal gasification in molten blast furnace slag. Industrial & Engineering Chemistry Research. 2012; 51(49): 15872-15883.

[102]   Mandapati RN, Daggupati S, Mahajani SM, Aghalayam P, Sapru RK, Sharma RK, and Ganesh A. Experiments and kinetic modeling for CO_2 gasification of Indian coal chars in the context of underground coal gasification. Industrial & Engineering Chemistry Research. 2012; 51(46): 15041-15052.

[103]   Zhang Y, Wu J, Chang L, Wang J, Xue S, and Li Z. Kinetic and thermodynamic studies on the mechanism of low-temperature oxidation of coal: A case study of Shendong coal (China). International Journal of Coal Geology. 2013; 120: 41-49.

[104]   Jing X, Wang Z, Zhang Q, Yu Z, Li C, Huang J, and Fang Y. Evaluation of CO_2 gasification reactivity of different coal rank chars by physicochemical properties. Energy & fuels. 2013; 27(12): 7287-7293.

[105]   Veca E and Adrover A. Isothermal kinetics of char-coal gasification with pure CO_2. Fuel. 2014; 123: 151-157.

[106]   Urych B. Determination of kinetic parameters of coal pyrolysis to simulate the process of underground coal gasification (UCG). Journal of Sustainable Mining. 2014; 13(1): 3-9.

[107]   Nunes K and Marcílio N. Determination of kinetic parameters of oxy-fuel combustion of coal with a high ash content. Brazilian Journal of Chemical Engineering. 2015; 32(1): 211-223.

[108]   Ding L, Zhou Z, Huo W, and Yu G. Comparison of steam-gasification characteristics of coal char and petroleum coke char in drop tube furnace. Chinese Journal of Chemical Engineering. 2015; 23(7): 1214-1224.

[109]   Chen C, Zhang S, Xu K, Luo G, and Yao H. Experimental and modeling study of char gasification with mixtures of CO2 and H2O. Energy & Fuels. 2015; 30(3): 1628-1635.

[110]   Tanner J and Bhattacharya S. Kinetics of CO_2 and steam gasification of Victorian brown coal chars. Chemical Engineering Journal. 2016; 285: 331-340.

[111]   Czerski G, Zubek K, Grzywacz P, and Porada S. Effect of Char Preparation Conditions on Gasification in a Carbon Dioxide Atmosphere. Energy & Fuels. 2017; 31(1): 815-823.

[112]   Liu L, Cao Y, Liu Q, and Yang J. Experimental and kinetic studies of coal−CO_2 gasification in isothermal and pressurized conditions. RSC Advances. 2017; 7(4): 2193-2201.

[113]   Zhang Y, Cai W, and Xin F. Simulation and Optimization of Coil Decoking in Ethane Pyrolysis Furnace. Chemical Engineering Communications. 2009; 196(8): 950-968.

[114]   Žajdlík R, Markoš J, Jelemenský Ľ, and Remiarová B. Single coal char particle combustion in the carbon dioxide atmosphere. Chemical Papers. 2000; 54(6b): 467-472.

[115]   Lee S, Speight JG, and Loyalka SK, Handbook of alternative fuel technologies. 2014: crc Press.

To whom correspondence should be addressed Dr. Ahmad Azari, Faculty of Petroleum, Gas and Petrochemical Engineering (FPGPE), Persian Gulf University (PGU), P.O. Box 75169-13817, Bushehr, Iran, e-mail address: azari.ahmad@gmail.com; azari.ahmad@pgu.ac.ir